Catalysis Today 174 (2011) 79–87

Contents lists available at ScienceDirect

Catalysis Today

journal homepage: www.elsevier.com/locate/cattod

Contrast on COD photo-degradation in coking wastewater catalyzed by TiO_2 and TiO_2–TiO_2 nanorod arrays

Min-Jiang Gao[a,*], Xi-Dong Wang[a], Min Guo[b], Mei Zhang[b]

[a] College of Engineering, Peking University, Beijing 100871, PR China
[b] Department of Physical Chemistry, University of Science and Technology Beijing, Beijing 100083, PR China

ARTICLE INFO

Article history:
Received 24 October 2010
Received in revised form 7 February 2011
Accepted 16 February 2011
Available online 5 April 2011

Keywords:
Coking wastewater
Photo-degradation
COD
TiO_2–TiO_2 nanorod arrays
Secondary structure

ABSTRACT

This paper deals with photo-degradation of chemical oxygen demand (COD) in coking wastewater catalyzed by TiO_2 nanorod arrays (TNAs) and special secondary structural TiO_2–TiO_2 nanorod arrays (TTNAs). The photo-catalysts, TNAs and TTNAs, were prepared by hydrothermal process and characterized by X-ray diffraction (XRD), field emission scanning electron microscope (FE-SEM) and high-resolution transmission electron microscopy (HRTEM). Well-aligned TNAs and TTNAs were prepared on the pretreated quartz substrates. It is proved that Rutile TiO_2 crystal seeds induce the nucleation and growth of TNAs preferably and the controllable synthesis of TTNAs with different secondary morphologies via hydrothermal approach could be achieved.

Chemical oxygen demand analyses, photochemical kinetic analysis and Fourier Transform infrared spectroscopy (FTIR) analysis have been carried out to obtain the details of the photo-catalytic degradation and mineralization of contaminants. The results show that these nanoscale catalysts exhibit high photocatalytic activities in degradation of COD in coking wastewater and TTNAs have significant advantages in COD removal. The optimum degradation efficiencies of COD reach 77.3% and 89.8% respectively using TNAs and TTNAs with catalyst addition of 0.04 g L^{-1} in 60 min reaction period. The effects of operating parameters on photo-degradation efficiency and the kinetics of COD photocatalytic degradation were investigated and discussed.

1. Introduction

Chemical oxygen demand (COD) is an important index of water quality. Organic pollutants present in wastewater are mainly characterized by COD, ammonia nitrogen (NH_3–N), total nitrogen (TN) and total phosphorus (TP). COD content indicates the amount of organic containments and hence water clean degree. Coking wastewater is a kind of typical industrial wastewater. It contains various refractory pollutants which still exist after conventional physical–chemical and biological treatments, such as phenol etc. Owing to their high biotoxicity, the organic compounds in coking wastewater are not readily degradable [1] and result in high content of COD. Compared with biological oxidation and chemical treatments, heterogeneous photocatalysis over TiO_2 have been proven to be effective for the removal of as-toxicants.

Titanium dioxide is non-toxic, photoetch-stable, inexpensive as one of the most effective semiconductor photocatalysts. Recently, it is reported that simultaneous removal of toxic pollutants in water can be realized via TiO_2-based photocatalytic reaction systems [2–4]. However, most applications in wastewater focus on TiO_2 powder and nanoparticles [5–7]. Compared with as-catalysts, TiO_2 nanorod/wire/tube arrays have relatively higher aspect ratio,lesser crystal interface, efficient charge separation, unique optical and electric properties. Therefore, TiO_2 nano arrays have been widely applied in many fields, including solar energy batteries, photocatalyst and gas sensors [8–10]. TiO_2 nano arrays, immobilized onto various supports, have improved properties in photocatalytic degradation of organic pollutants [11,12], water photoelectrolysis [13,14] and etc., with the improvement of complicated separation performance of TiO_2 power. Many approaches have been reported to fabricate TiO_2 nano arrays, such as template-assisted method, electrochemical anodic oxidation method, chemical vapor deposition and hydrotheimal method [15–18]. Among them, hydrothermal synthesis of TiO_2 nano arrays is a promising process due to simple control, quick reaction and relatively low cost. However, preparing TiO_2 nano arrays via hydrothermal approach is rarely reported. Zhang et al. [11] synthesized TiO_2 nanotape arrays via hydrothermal reaction in NaOH solution on a modified Ti foil which was pre-coated with anatase titania particles as seeds. The seed-induced hydrothermal method improves the growth density and diameter distribution of TiO_2 nanotape array, however, the growth orientation and morphologies related to the photocatalytic

* Corresponding author. Tel.: +86 010 62756623; fax: +86 010 62756623.
E-mail address: gaominjiang@pku.edu.cn (M.-J. Gao).

0920-5861/$ – see front matter © 2011 Elsevier B.V. All rights reserved.
doi:10.1016/j.cattod.2011.02.024

ability of TiO_2 nano arrays are not ideal. In application, it is effective and important for TiO_2 nano arrays to obtain uniform density distribution and well-aligned orientation, especially utilized as solar cells and photocatalyst. Wu et al. [19] produced a unique nanostructured titania film consisting of crystalline nanopillars for the first time via structural transformation of a 3D hexagonal phase. The film of crystalline TiO_2 nanopillars with inverse mesospace is expected to have potential applications for photocatalysts and optical-electronic devices. Recently, Wang et al. [20] reported that single-crystalline rutile TiO_2 nanorod arrays were grown on Si substrates and FTO-covered glass by a mild hydrothermal process. The prepared dye-sensitized solar cells, assembled with the single-crystalline rutile TiO_2 nanorod arrays, grown on FTO-covered glass as photoanode show a power conversion efficiency (1.10%). The proposed method may be further extended to the synthesis of other 1D nanostructures arrays with similar crystal structures. Similarly, for the formation of new solar cells, Wang et al. [21] fabricated a CdS quantum dots-sensitized single-crystalline rutile TiO_2 nanorod array on FTO substrate photoelectrodes by a simple chemical method. The photoelectrodes allow more incident light to pass through the back side of FTO substrates to induce more CdS quantum dots to generate photoelectrons and can efficiently separate and transfer photogenerated electrons from CdS quantum dots to the collected FTO substrates. The photoelectrochemical properties of the as-prepared arrays achieved are comparable to those of CdS quantum dots-sensitized TiO_2 nanotube array, suggesting that the TiO_2 nanorod array has a potential application in solar cells.

According to the studies above, the photoconversion efficiency has been enhanced by well-oriented TiO_2 nanorod array sensitized via dye or else, but investigations on the application in the field of wastewater treatment are still rarely reported.

In this present work, well-aligned TiO_2 nanorod arrays (TNAs) and TiO_2-TiO_2 nanorod arrays (TTNAs) were prepared on the pretreated quartz substrates. The introduction of TiO_2 crystal seeds on the substrate has a great influence on the morphologies and the alignment ordering of TNAs and consequently TTNAs. TTNAs are novel nanomaterials synthesized in our laboratory with unique secondary structure by hydrothermal process. Photo-degradation efficiencies of COD in coking wastewater catalyzed by TNAs and TTNAs were evaluated by in a self-design fluidized bed photoreactor. The effects of parameters on COD degradation efficiency were investigated and the kinetics was analyzed. In addition, the total oil of coking wastewater before and after photocatalytic reactions was identified through FTIR analysis.

2. Experimental

2.1. Preparation of TNAs and TTNAs by hydrothermal method

Tetrabutyl titanate was dissolved in the mixed solution of ethanol and diethanolamine, keeping the mol ratio of tetrabutyl titanate and diethanolamine at 1:1, and stirred for 60 min. The mixed solution of 1.7 mL deionized water, 34 mL ethanol and 0.13 mL hydrochloric acid (37% HCl) was dropwise added to the above solution and further violently stirred for 15 min, then aged for 24 h at room temperature to obtain a homogeneous and stable TiO_2 colloid solution. The as-prepared pre-coating solution was then dropped and spun onto the quartz substrates using spin coater (KW-4A, made by the Chinese Academy of Sciences) at the rate of 3000 rpm for 30 s. The substrates were dried and heat-treated at 800 °C for 15 min in muffle furnace. The process was repeated for three times and thus the pretreated substrates were prepared. Subsquently, 0.05 M $TiCl_3$ precursor solution, in which NaCl was added to and keeping it saturated, was poured into a sealed Teflon autoclave. The pretreated substrate was slantwise immersed in the precursor solution. The hydrothermal reaction was carried out at 190 °C for 3 h. After the reaction, the substrate was rinsed with deionized water and dried at room temperature. TNAs were prepared. Finally, the preparation of TTNAs was proceed using the same mixture of $TiCl_3$ solution and NaCl under the above conditions except the pH was set to 1.20.

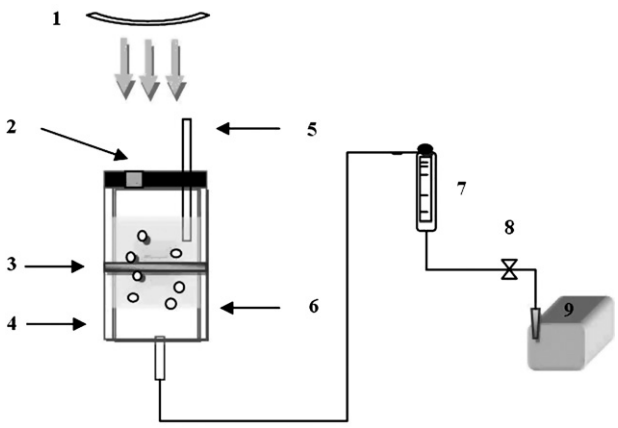

Fig. 1. Photochemical reactor for coking wastewater degradation: (1) 300 W UV light;(2) air outlet;(3) interlayer;(4) air cell;(5) sampling hole;(6) micro-pore titanium plate;(7) rotameter;(8) air valve;(9) air pump.

2.2. Photocatalytic degradation of COD experiment

The photocatalytic activities of TNAs and TTNAs were evaluated through photo-degradation of COD in coking wastewater in a fluidized bed photoreactor (see Fig. 1). The main part of photocatalysis reactor was a quartz column of 260 mm height and 60 mm inner diameter, separated into the main chamber for photocatalytic reactions and the air cell by a micro-pore titanium plate. The demountable interlayer set in the main chamber was used for regulation of catalyst setting position in catalytic processes. The photocatalytic reaction solutions were illuminated by the 300 W UV light (250–380 nm, Beijing Bofeilai Technology Co., Ltd.) over the chamber. The coking wastewater was sampled from an iron and steel plant. The composition of raw coking wastewater is listed in Table 1.

The photo-degradation of COD was carried out with the catalyst addition of 0.004 g L^{-1} or 0.04 g L^{-1} and aerated from the bottom air chamber. The air flow rate was adjusted to 5 L min^{-1}. All reactions were conducted in the temperature range of 25–30 °C and the reaction period of 60 min. The solution samples were collected at the given irradiation time intervals and then filtered prior to analysis for separation of the suspended solid.

2.3. Analytical Methods

The as-prepared TNAs and TTNAs crystal structures were characterized by X-Ray diffraction (XRD) performed on a D/MAX-PC 2500 diffractometer with Cu-Kα radiation (40 kV, 100 mA). The

Table 1
Organic components of raw coking wastewater.

Component	COD	NH_3–N	Organic substances
Content (mg/L)	2030	296.8	Phenols, Phenyls, Organic nitrogen, Naphthalin, Anthracene

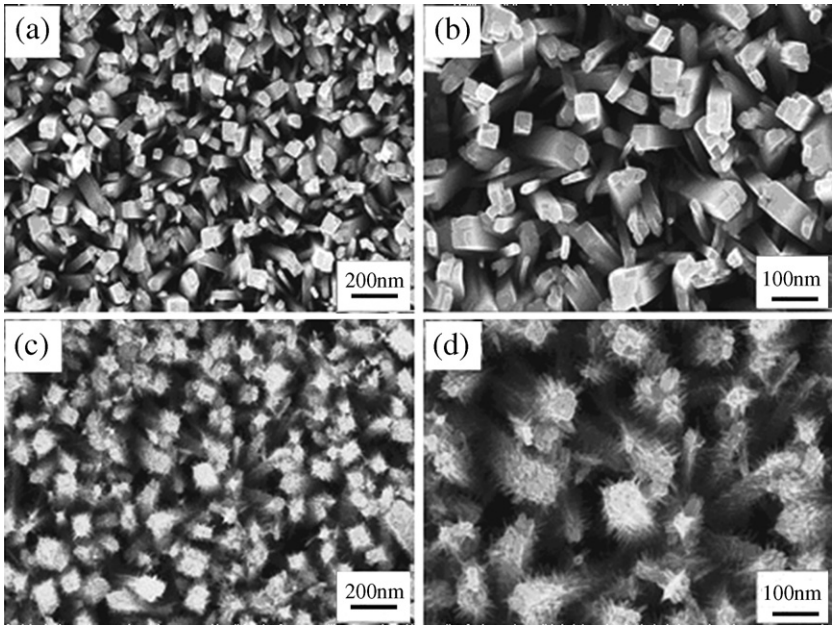

Fig. 2. SEM image of the nano photo-catalysts: (a) (b) TiO_2 nanorods;(c) (d) TiO_2–TiO_2 nanorods (secondary structure).

Raman spectra was recorded on a laser Raman micoscpoe system (Renishaw RM-1000) with the accuracy in the Raman shift estimating to be ~0.5 cm^{-1}. The morphologies of catalysts and the special secondary structure of TTNAs were investigated by field-emission scanning electron microscopy (FE-SEM, ZEISS SUPRA^{TM}55 operated at 10 keV) and high-resolution transmission electron microscopy (HRTEM, H-9000 NAR at 300 kV).

Gas chromatography-mass spectrometry (GC–MS, TraceDSQ) has been carried out to obtain the details of the composition of raw coking wastewater. The transparent solution samples before and after photo-degradation reactions was analyzed by Fourier Transform infrared spectroscopy (FTIR, VECTOR22, Bruker). The COD concentration was evaluated by potassium dichromate method [7,22–26].

3. Results and discussion

3.1. Morphologies and crystal structure characterization of TNAs and TTNAs

Fig. 2 shows the SEM images of TiO_2 nanorods arrays (TNAs) and TiO_2–TiO_2 nanorod arrays (TTNAs) grown on the quartz substrates. Fig. 2(a) and (b) reveal that high density, well ordered and uniform TNAs were prepared on the pretreated substrates, while the special secondary structure of TTNAs (brushes like) is shown in Fig. 2(c) and (d).

Table 2
Comparison on the the aspect ratio of TNAs and TTNAs.

	Core rod diameter (nm)	Burr-like rod diameter (nm)	Core rod length (nm)
TNAs	80–90	–	1700
TTNAs	100–110	20–30	2200

The side view of novel photocatalysts (TTNAs) is performed in Fig. 3. The average diameter and length of TiO_2–TiO_2 nano core rods are about 100 nm and 2200 nm, respectively, with burr-like rods average diameter of 20–30 nm. Table 2 performs comparison on the aspect ratio of TNAs and TTNAs.

Fig. 4 shows low-magnification TEM and HRTEM images of an individual TiO_2–TiO_2 nanorod. The images demonstrate that the TiO_2–TiO_2 nanorod arrays (TTNAs) were successfully synthesized with brushes-like special secondary structure. The clear lattice fringes indicate that TiO_2–TiO_2 nanorod is well crystallized. The spacing between two fringes is 0.32 nm and consistent with the interplanar distance of the (1 1 0) planes of the standard rutile TiO_2. It can be seen that the (1 1 0) fringes parallel to the *c*-axis of nanorods, suggesting that the core and the burr-like ones of TiO_2–TiO_2 nanorods both grow along the [0 0 1] direction. According to literature reports, the (1 1 0) plane has the lowest surface energy among the surfaces of rutile TiO_2 [27]. The planes with low surface energies generally grow slowly and tend to survive during

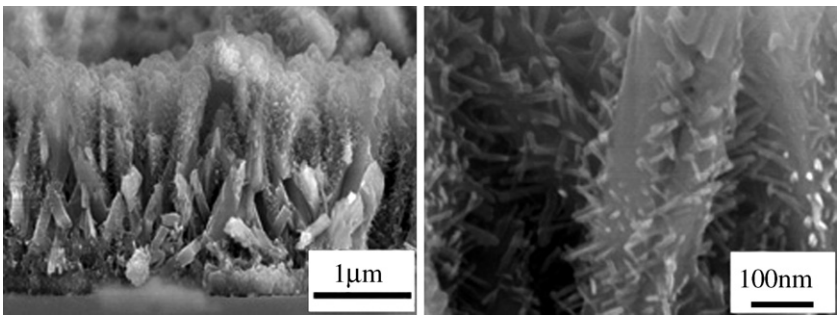

Fig. 3. SEM side view of TiO_2–TiO_2 nanorods (secondary structure).

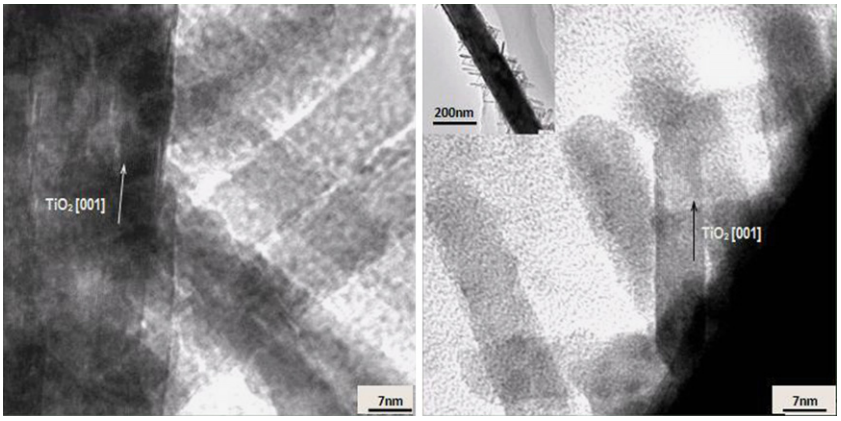

Fig. 4. TEM and HRTEM images of TiO_2–TiO_2 nanorod: (a) high-magnification image of the core rod, and (b) high-magnification image of the burr-like rods. Inset in (b): the corresponding low-magnification image of the TiO_2–TiO_2 nanorod.

the growth [28], and thus the (1 1 0) plane is obviously observed in the HRTEM images. Furthermore, Cl^- in the precursor solution is preferentially absorbed onto the (1 1 0) surface and retard its growth rate. As a result, it greatly promotes the growth of the core and the burr-like ones of TiO_2–TiO_2 nanorods along the [0 0 1] direction [29–31]. In addtion, according to the TEM and HRTEM images, it can be seen that the burr-like rods grew around the main core rod, resulting in inter-overlapping screenages and focus differences. The results are in accordance with SEM images observations.

The XRD patterns of the quartz substrate, the pretreated substrate (TiO_2 crystal seeds), TNAs and TTNAs are shown in Fig. 5(left). The results indicate that TNAs (Fig. 5(c)) and TTNAs (Fig. 5(d)) were found to be crystalline and identified by diffraction peaks belonging to rutile. A number of researches [32–35] reported that the synthesized TiO_2 nanorods via hydrothermal approach in strongly acidic solution are usually pure rutile phase, which is in consistent with the XRD results in this paper. Compared with the pattern of the pretreated substrate (Fig. 5(b)), the intensity of TNAs and TTNAs diffraction peaks was relatively higher indicating the perfect crystallization of as-prepared catalysts induced by rutile TiO_2 crystal seeds. The narrower diffraction lines of TTNAs show that the average size of nanorods was somewhat larger than that of TNAs. The broad base lines observed in XRD patterns of Fig. 5(b)–(d) demonstrate the presence of small quantity of amorphous phase [36]. The Raman spectrum of TTNAs was shown in Fig. 5(right), reproducing the existing literature data [37] with the bands at 143 cm^{-1} (weak), 447 cm^{-1} (strong), 612 cm^{-1} (strong) and a combination band at 235 cm^{-1} (medium). The bands observed are consistent with the ones observed for rutile TiO_2 and also in accordance with the XRD pattern of TTNAs (left (d)).

3.2. The photo-degradation of COD in coking wastewater catalyzed by TNAs and TTNAs

To find out the optimal conditions of COD decomposition, the solution pH was investigated in the range of 2.0–10.0 and the light intensity of UV irradiation with different addition amount of catalysts was studied as well.

The pH value in the reaction system exhibits significant influence on TiO_2 surface charge and adsorption ability [1,38]. The effect of pH on the COD degradation efficiency is presented in Fig. 6. The amount of TNAs and TTNAs was fixed as 0.004 g L^{-1} respectively, the air flow rate as 5 L min^{-1}, the temperature as 25–30 °C and the degradation reaction time as 60 min. The results show that the decomposition rates of COD increased when the solution pH increased from 2.0 to 7.0 (natural pH value), while the degradation efficiencies went down when the pH was adjust to 8.0. The optimal solution pH value for COD photo-degradation was 7.0, which was similar to that reported by other work [7]. Compared with the degradation curve catalyzed by TNAs, the one with TTNAs fed into the reaction solutions takes on higher degradation due to better aspect ratio and probability of more reactive sites induced by UV irradiation.

The surface reactions of catalysts are expected to occur as follows at different pH values, which is based on the zero charge point

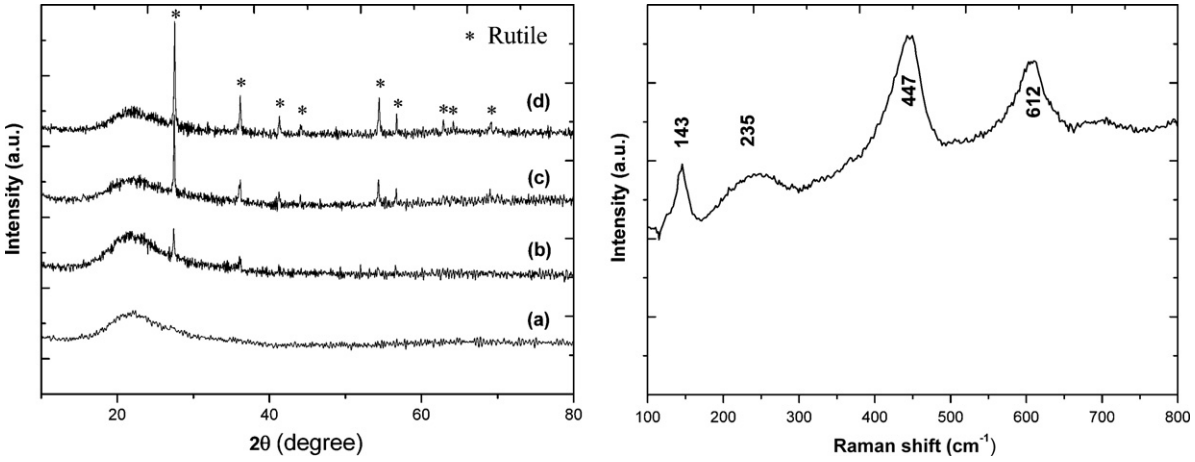

Fig. 5. XRD patterns (left): (a) the quatz substrate; (b) the pretreated substrate; (c) TNAs; (d) TTNAs, and Raman spectrum (right) of TTNAs.

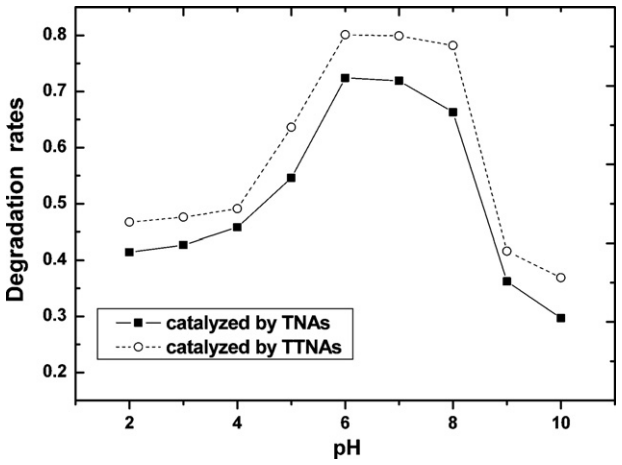

Fig. 6. The effect of solution pH value on COD photo-degradation (UV intensity = 400 mW cm^{-2}; air bubble volumns: 5 L min^{-1}; [TNAs or TTNAs] = 0.004 g L^{-1}).

of TiO_2 (pH_{pzc} 6.25) [1,39]:

$$pH < pH_{pzc}: TiOH + H^+ \rightarrow TiOH_2^+ \quad (1)$$

$$pH > pH_{pzc}: TiOH + OH^- \rightarrow TiO^- + H_2O \quad (2)$$

It is proved that the electrical charge of components in coking wastewater and the TNAs or TTNAs surface determines the adsorption content and effect. When the solution pH was set in the lower range of 2.0–6.0, the degradation ratios of COD catalyzed by TNAs and TTNAs increased and reached 72.4% and 80.1% as the maxima at the pH value of 6.0. However, the efficiencies decreased with the rising of pH value in the higher range of 7.0–10.0. The results reveal that the composition of coking wastewater might be negatively charged or perform as electroneutrality molecules in acidic media, which was effective to adsorption on the surface of catalysts positively charged. For pH 2.0–4.0, the slight lower degradation rates of COD were attributed to the Cl^- ions introduced by HCl used for pH regulation. According to some reports [40–42], the Cl^- ions and the substances in coking wastewater solutions might have an adsorption competition on the surfaces of TNAs and TTNAs, resulting in decrease of catalytic activity. At the point of neutral pH value (6.0–7.0), the highest photo-degradation rate was reached due to the optimal adsorption content. It can be explained by the less and absence of Cl^- ions with little addition of HCl. The pH value of raw coking wastewater was examined as 7.17. In alkaline conditions (pH value from 8.0–10.0), the majority of contamination exsiting in solutions was still probably charged negatively, and thus the adsorption was profoundly influenced by the TiO^- increased on the surfaces of TNAs and TTNAs. In addition, the Na^+ and OH^- ions were also proved to initiate adsorption competition [42], consequently decreasing the degradation efficiencies of COD.

The effect of UV intensity on the photo-degradation of COD was investigated. According to the results above, the pH was fixed to the neutral value of 7.17 in coking wastewater solutions, which was measured before. The temperature was still maintained as 25–30 °C with the flow rate kept 5 L min^{-1}. During the same reaction period of 60 min, the light intensity and the addition amount of TNAs or TTNAs were examined as important factors to efficiencies of COD photocatalytic degradation. Fig. 7 shows the COD concentration as a function of reaction time under different condition combinations of light intensities and the contents of catalysts fed into the solutions. The degradation rates effectively increased with

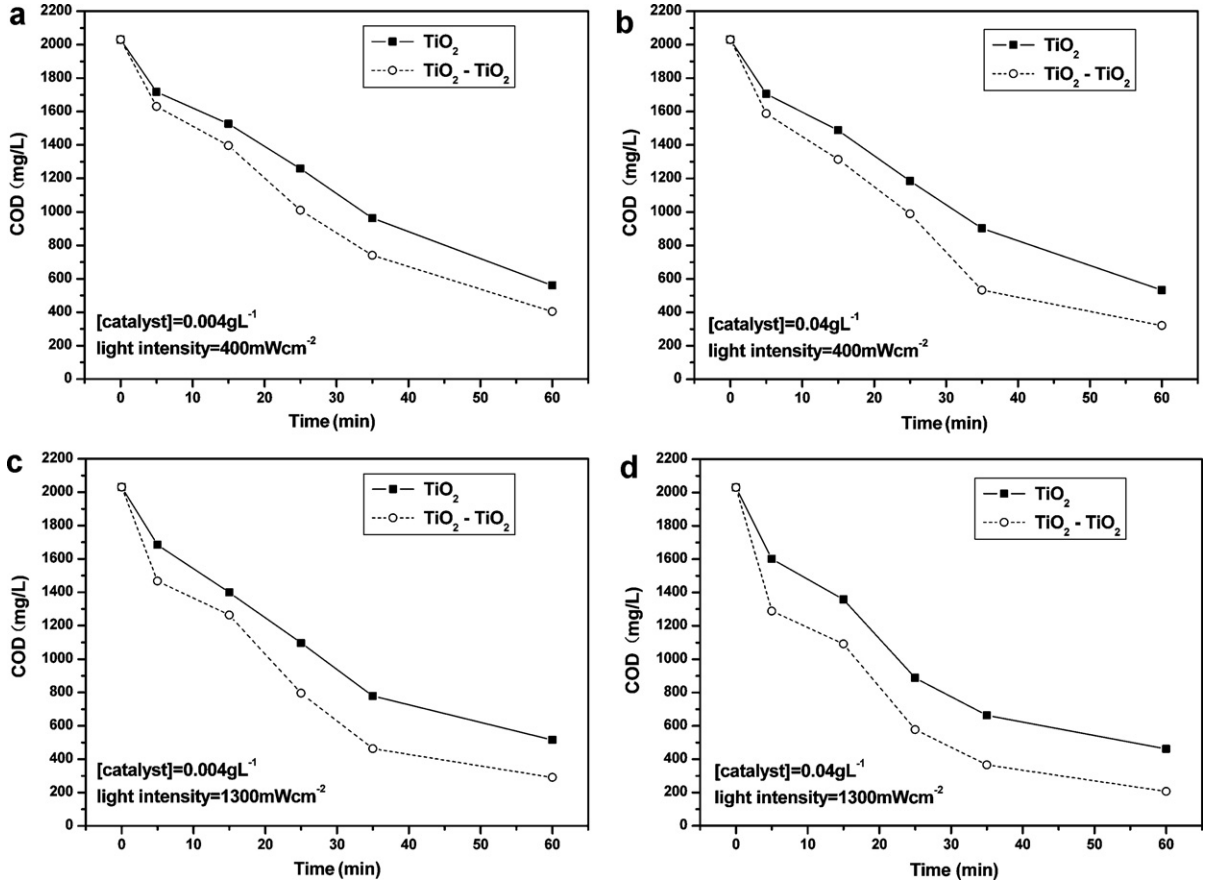

Fig. 7. Parameters effect on COD degradation catalyzed by TNAs and TTNAs.

Table 3
The value of k_{app} and R^2 in different reaction conditions.

Parameter combination ($g\,L^{-1}$, $mW\,cm^{-2}$)		Kinetics equations	k_{app} (min^{-1})	R^2
TNAs	0.004, 400	$\ln(C_0/C_t) = 0.0211t + 0.0022$	0.0211	0.9964
	0.04, 400	$\ln(C_0/C_t) = 0.0221t + 0.0142$	0.0221	0.9978
	0.004, 1300	$\ln(C_0/C_t) = 0.0230t + 0.0473$	0.0230	0.9931
	0.04, 1300	$\ln(C_0/C_t) = 0.0251t + 0.0920$	0.0251	0.9808
TTNAs	0.004, 400	$\ln(C_0/C_t) = 0.0267t + 0.0292$	0.0267	0.9973
	0.04, 400	$\ln(C_0/C_t) = 0.0314t + 0.0318$	0.0314	0.9865
	0.004, 1300	$\ln(C_0/C_t) = 0.0330t + 0.0900$	0.0330	0.9825
	0.04, 1300	$\ln(C_0/C_t) = 0.0379t + 0.1696$	0.0379	0.9799

the increase of UV intensities, the catalysts addition and the both parameters, respectively. Compared with TNAs, TTNAs as catalysts created higher photo-degradation ratios of COD in the same reaction systems with the fixed addition amount of 0.004 g L^{-1} (Fig. 7(a), (c)) or 0.04 g L^{-1} (Fig. 7(b), (d)) and the UV light intensities set to 400 mW cm^{-2} (Fig. 7(a), (b)) or 1300 mW cm^{-2} (Fig. 7(c), (d)). The efficiency differences observed demonstrate that the UV light intensity and the contents of catalysts addition play a positive role in COD photo-degradation and the combination of the two parameters can enhance the photocatalytic activities remarkably. The maxima of corresponding degradation ratios reached 77.3% and 89.8% using TNAs and TTNAs as catalysts respectively. The comparison of degradation curves between Fig. 7(b) and (c) reveals that the as-prepared TNAs and TTNAs have greatly photocatalytic abilities. The catalytic potential of TTNAs in the applications of any organic pollutant is expected as well as TNAs.

The findings in Fig. 7 can been explained by the following reasons. TNAs and TTNAs absorbed more photons with the increase of UV light intensity, and subsequently more active sites were created, where the hydroxyl radicals (OH•) and superoxide radical anion ($O_2^{-\bullet}$) were induced to enhance the efficiencies of COD photo-degradation. When the amount of UV light was fixed with irradiation time kept in constant, the hydroxyl radicals (OH•) and superoxide radical anion ($O_2^{-\bullet}$) generated at the reactive sites also held the fixed values on the surfaces of TNAs and TTNAs. More catalysts set into the solution systems introduced more sites to absorb the photons provided by UV light, resulting in the higher degradation ratios of COD from coking wastewater. In additon, UV light intensity and catalyst amount have a little different effect upon the reaction rates over TNAs and TTNAs. It might be speculated that high activity and COD decomposition rate are attributed to efficient charge separation and transport properties of rutile-crystalline structures of both TNAs and TTNAs as well as superior light harvesting efficiency via the quartz substrates, while the differences between the two catalyst are probably resulted in by the intervention of TTNAs sub-structure. The interface between TiO_2–TiO_2 nano core rods and burr-like rods might be suitable for defect formation,which is effective to separation of the photo-induced exciton. Thus, TTNAs performed to be more active during the reactions than TNAs in the same conditions.

Fig. 8 exhibits the linear plot of $\ln(C_0/C)$ against reaction time corresponding to the results in Fig. 7. The apparent rate constants (k_{app}, min^{-1}) and correlation coefficient (R^2) were determined by linear regression. The data is listed in Table 3 with the linear regression equations.

It can be found that, according to many literatures, the kinetics analysis of heterogeneous photocatalytic reactions is in accordance with pseudo-first-order or first-order kinetics models, commonly described as equation (3).

$$-r_A = -\frac{dC_A}{dt} = kC_A$$
$$C_A = C_{A_0} e^{-kt} \quad (3)$$

However, the present work in our research (see Table 3: R^2 et al.) indicates that some of the photo-degradation reactions of COD, catalyzed by TNAs and TTNAs, fitted not well with the pseudo-first-order and first-order kinetics, or some of degradation analyses did not obey the models. The results might be attributed to the complex composition of coking wastewater and the special unclear variations of COD photo-degradation end products, intermediate products and reaction process. Further investigation is in progress.

The effect of UV light intensity only on COD photodegradation was studied by using strong UV light of 400 mW cm^{-2} and 1300 mW cm^{-2} without catalysts. Fig. 9 shows the COD concentration as a function of irradiation time under the two different light intensities. The blank test result performs that COD degradation ratio can be affected via strong UV light, which resulting in COD degradation rates of 17.8% (UV intensity = 400 mW cm^{-2}) and 31.2%(UV intensity = 1300 mW cm^{-2}). It can be calculated that the light intensity contributes 21.1% and 34.7% degradation ratios

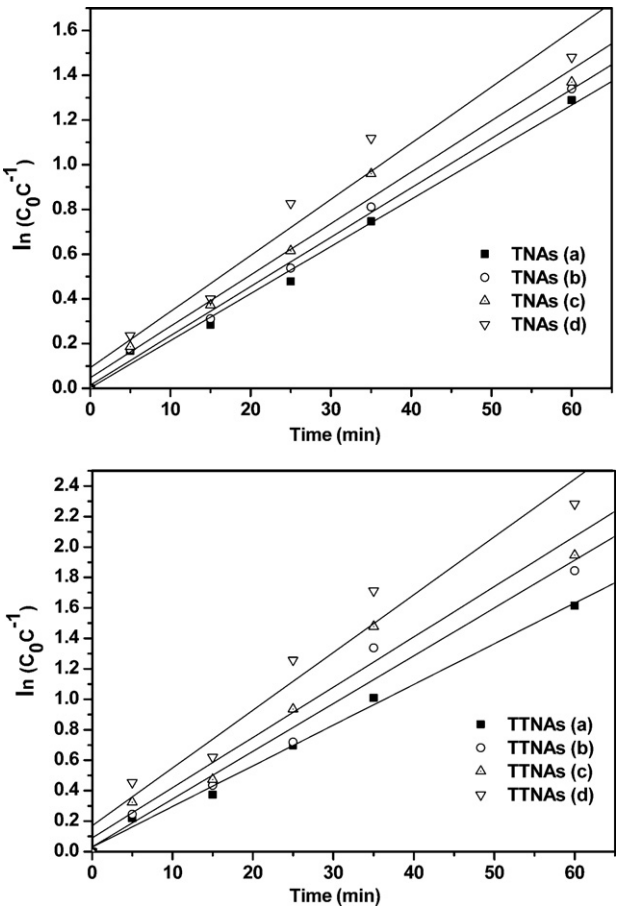

Fig. 8. Kinetic analysis of COD photo-degradation with different parameter combinations using TNAs and TTNAs.

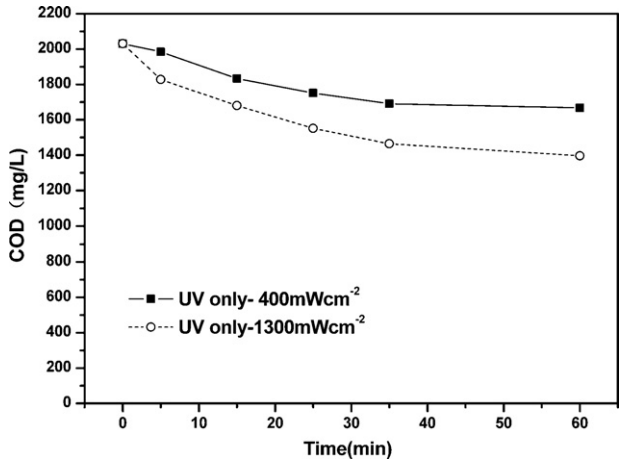

Fig. 9. The COD degradation rates against reaction time without TNAs and TTNAs: (air bubble volumns: 5 L min^{-1}; pH 7.17; UV intensity = 400 mW cm^{-2}/1300 mW cm^{-2}).

to optimal COD removal by TTNAs ([TTNAs] = 0.04 g L^{-1}), with the intensity fixed as 400mW cm^{-2} and 1300 mW cm^{-2}, respectively.

Standard TiO_2 nanoparticles (Degussa P25) were used for comparison. The pH was fixed to the neutral value of 7.17 in coking wastewater solutions. The temperature was kept at 25–30 °C with the flow rate adjusted to 5 L min^{-1}.The addition amount of TNAs, TTNAs, P25 and were fixed as 0.004 g L^{-1}, 0.004 g L^{-1} and 0.02 g L^{-1} respectively. During the same reaction period of 60 min, the degradation rates of COD were expressed in Fig. 10. TiO_2 nanoparticles (Degussa P25) have a diameter of approximately 21 nm, and the specific surface area is about 51.2 m^2/g. It is calculated that the degradation rate of COD in coking wastewater after 60 min reached 72.4%, 73.8% and 80.1% catalyzed by TNAs, P25 and TTNAs, respectively. The results indicate that TNAs and P25 have similar degradation rates. However, considering the mass of TNAs and TTNAs are far less than that of P25, it can be concluded that TNAs and TTNAs have a higher photocatalytic activity than P25. The excellent photocatalytic activity of TNAs and TTNAs may be attributed to the single crystal structure of TNAs and the unique secondary structure of TTNAs, resulting in the efficient the transmission of photogenerated electron and hole.

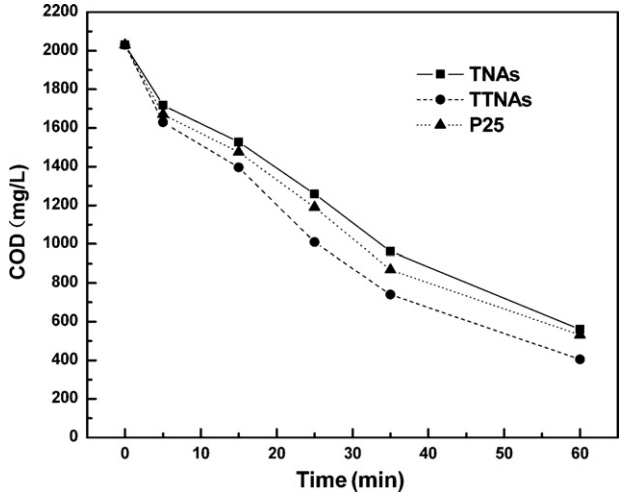

Fig. 10. Photodegradation rate curves of COD. (UV intensity = 400 mW cm^{-2}; air bubble volumns: 5 L min^{-1}; pH 7.17; [TNAs/TTNAs/P25] = 0.004 g L^{-1}/0.004 g L^{-1}/0.02 g L^{-1}).

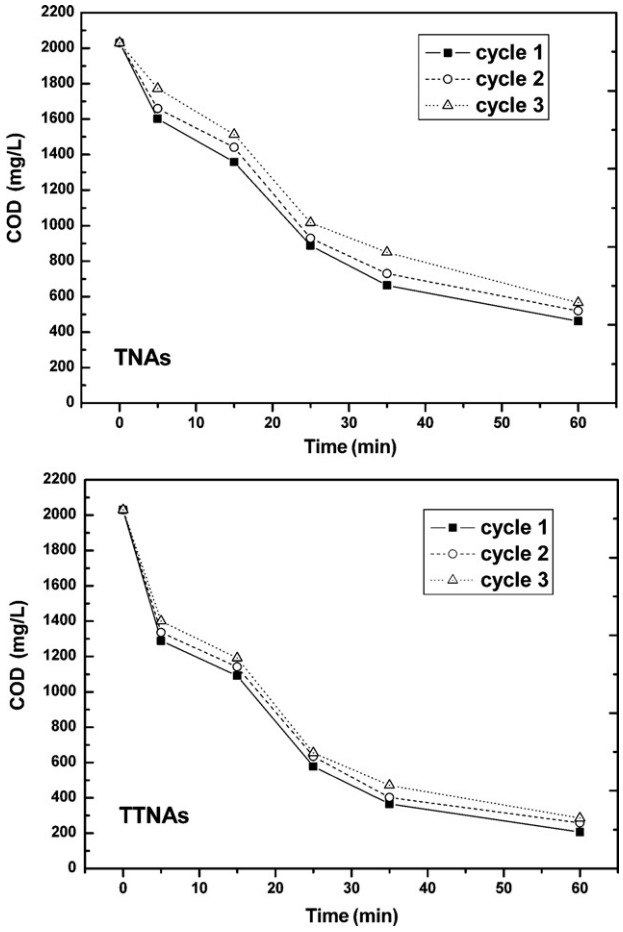

Fig. 11. The COD degradation rates against reaction time catalyzed by recycled TNAs and TTNAs (UV intensity = 1300 mW cm^{-2}; air bubble volumns: 5 L min^{-1}; pH 7.17; [initial TNAs or TTNAs] = 0.04 g L^{-1}).

Finally, recycling tests were operated to evaluate the repeatability of TNAs and TTNAs with the optimal reaction conditions fixed in each cycle. Fig. 11 performs the degradation efficiencies of COD only reduced 5.2% (TNAs) and 3.9% (TTNAs) after 3 cycles. The results demonstrate that the photocatalytic activities of catalysts prepared in this paper are significantly higher and TTNAs have better repeatability, compared with TNAs. The solid carrier has a positive effect on the recycle of catalysts and the efficiencies of COD degradation, due to the less loss than that of TiO_2 nanoparticles in the reaction processes and recycling experiments.

3.3. The photcatalytic decomposition of total organic pollutants in coking wastewater

The total contamination in coking wastewater, initiating high content of COD, was identified and measured by Fourier Transform infrared spectroscopy (FTIR) analysis based on potassium dichromate method [7,22–26]. The FTIR spectra before and after photocatalytic reaction catalyzed by TTNAs in the optimal conditions are shown in Fig. 12(a) and (b).

The infrared spectrum of composition before degradation (Fig. 12(a)) shows the bands at 3610 cm^{-1} (strong), 3397 cm^{-1} (strong), 1642 cm^{-1} (medium) and 791 cm^{-1} (medium). Compared with the above results, the bands attributed to the end products after decomposition presented in Fig. 12(b) are observed at 3651 cm^{-1} (weak), 1654 cm^{-1} (weak) and 795 cm^{-1} (strong, spike) with variations in the positions observed in Fig. 12(a). The results demonstrate the total content of contaminants decreased dra-

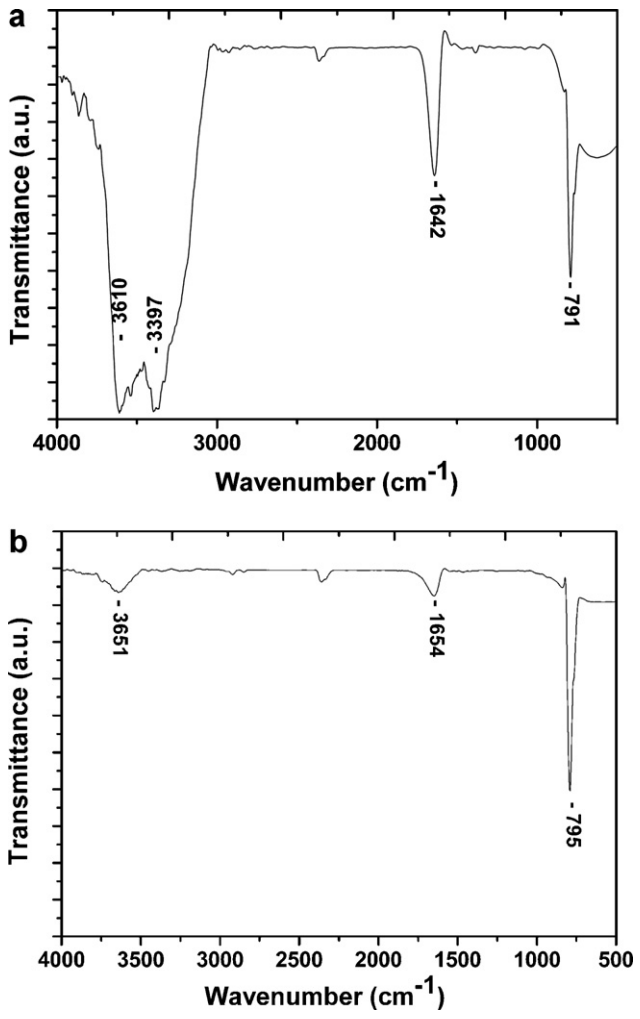

Fig. 12. FTIR spectrum of components in coking wastewater before and after mineralization catalyzed by TTNAs (UV intensity = 1300 mW cm^{-2}; air bubble volumns: 5 L min^{-1}; pH 7.17; [TTNAs] = 0.04 g L^{-1}).

matically after a reaction period of 60 min. The concentrations of substances, the initial peaks of which at 3610 cm^{-1}, 3397 cm^{-1} and 1642 cm^{-1}, reduced remarkbly, while the content of pollutants with initial band at about 791 cm^{-1} was enhanced.

According to the FTIR standard spectra [43–45], the results can be analyzed as follows: the band at 3610 cm^{-1} is due to O–H stretching mode of phenolic hydroxyl and alcoholic hydroxyl groups; the band at 3397 cm^{-1} belongs to N–H stretching mode of amine group; the bands at 1642 cm^{-1} and 791 cm^{-1} are attributed to aromatic skeleton vibration (related to pyridine, furan, quinoline and benzene) and C–H deformation mode of substituted benzene groups, respectively. Therefore, it can be found that the majority of phenols, amine, benzene, pyridine, furan and quinoline etc. are mineralized completely by TTNAs. The total content of substituted benzene (bands at 910–670 cm^{-1}) also decreases, while the amount of m-dimethyl substituted benzene 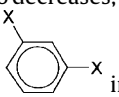 increases remarkbly with the content declines of p-dimethyl substituted benzene  , o-dimethyl substituted benzene 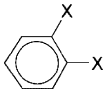 and other substituted benzene 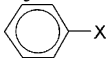 .

4. Conclusions

Well-aligned TiO_2 nanorod arrays (TNAs) and TiO_2–TiO_2 nanorod arrays (TTNAs) have been prepared by a facile hydrothermal preparation method. TTNAs are synthesized as a novel nanomaterial with special brushes-like secondary structure. The TNAs and TTNAs growth can be controled by the precusor solution pH value and pre-coating rutile TiO_2 seeds on the quartz substrates. The as-prepared TNAs and TTNAs have great photocatalytic activities, resulting in the maxima of COD degradation as 77.3% and 89.8% respectively, with the optimal combination conditions of UV light intensity as 1300 mW cm^{-2}, the flow rate as 5 L min^{-1}, solution pH value as 7.17, the catalysts addition of 0.04 g L^{-1} and the reaction temperature as 25–30 °C. According to the comparisons between the degradation curves catalyzed by TNAs and TTNAs, the ones with TTNAs fed into the reaction solutions present higher degradation efficiencies due to better aspect ratio and probability of more reactive sites induced by UV irradiation. The FTIR spectrum shows the composition variation of total organic pollutants in coking wastewater and reveals that the majority of contaminants were mineralized by TTNAs after photo-degradation reaction.

This work may be developed to a general way to prepare TNAs and TTNAs on substrates in a larger scale and realize the high repeatability of catalysts, which are potentially applied in photodegradation of any pollutants in coking wastewater. Further study is in progress.

Acknowledgement

The authors thank the National Natural Science Foundation in China for supporting this research under the grant of no. 50772004.

References

[1] Sze-Mun Lam, Jin-Chung Sin, Abdul Rahman Mohamed, Kor. J. Chem. Eng. 27 (4) (2010) 1109–1116.
[2] P.R. Gogate, A.B. Pandit, Adv. Environ. Res. 8 (2004) 501.
[3] R. Thiruvenkatachari, S. Vigneswaran, I.S. Moon, Kor. J. Chem. Eng. 25 (2008) 64.
[4] Y.J. Chen, E. Stathatos, D.D. Dionysiou, J. Photochem. Photobiol. A: Chem. 203 (2009) 192.
[5] X. Liu, F.T. Liu, N. Zhang, et al., Bull. Chin. Ceram. Soc. 25 (6) (2006) 135–139.
[6] N. Frank, A.J. Bard, J. Am. Chem. Soc. 99 (1) (1977) 303–304.
[7] LiuWen Xiu, Liu Qing, Li Xiu Fang, Song Yun Ting, Cao Wen Bin, Sci. Chin.Technol. Sci. 53 (2010) 1477–1482.
[8] X.H. Xia, Y.S. Luo, Z. Wang, Y. Liang, J. Fan, Z.J. Jia, Z.H. Chen, Mater. Lett. 61 (2007) 2571.
[9] G.K. Mor, K. Shankar, M. Paulose, O.K. Varghese, C.A. Grimes, Nano Lett. 6 (2006) 215.
[10] I.D. Kim, A. Rothschild, B.H. Lee, D.Y. Kim, S.M. Jo, H.L. Tuller, Nano Lett. 6 (2006), 2009.
[11] Q. Zhang, A.K. Chakraborty, W.I. Lee, J. Phys. Chem. Solids 69 (2008) 1450–1453.
[12] H.C. Liang, X.Z. Li, J. Hazard. Mater. 162 (2009) 1415–1422.
[13] E.Y. Kim, J.H. Park, G.Y. Han, J. Power Sources 184 (2008) 284–287.
[14] Z.Y. Liu, B. Pesic, K.S. Raja, R.R. Rangaraju, M. Misra, Int. J. Hydrogen Energy 34 (2009) 3250–3257.
[15] W. Ho, J.C. Yu, J.G. Yu, Langmuir 21 (2005) 3486.
[16] M. Paulose, K. Shankar, S. Yoriya, H.E. Prakasam, O.K. Varghese, G.K. Mor, T.A. Latempa, A. Fitzgerald, C.A. Grimes, J. Phys. Chem. B 110 (2006) 16179.
[17] S.K. Pradhan, P.J. Reucroft, F.Y. Dozier, J. Cryst. Growth 256 (2003) 83.
[18] Z.R. Tian, J.A. Voigt, J. Liu, B. Mckenzie, H. Xu, J. Am. Chem. Soc. 125 (2003) 12384.
[19] C.W. Wu, T. Ohsuna, M. Kuwabara, K. Kuroda, JACS 128 (2006) 4544.
[20] H.E. Wang, Z.H. Chen, Y.H. Leung, C.Y. Luan, C.P. Liu, Y.B. Tang, C. Yan, W.J. Zhang, J.A. Zapien, I. Bello, S.T. Lee, Appl. Phys. Lett. 96 (2010) 263104.
[21] H. Wang, Y.S. Bai, H. Zhang, Z.H. Zhang, J.H. Li, L. Guo, J. Phys. Chem. C 114 (2010) 16451.
[22] L.R. Pitwell, Chem. Brit. 19 (1983) 907.
[23] W.A. Moore, R.C. Kroner, C.C. Ruchhoft, Anal. Chem. 21 (1949) 953.
[24] A.I. Medalla, Anal. Chem. 23 (1951) 1318.
[25] W.A. Moore, F.J. Ludzack, C.C. Ruchhoft, Anal. Chem. 23 (1951) 1297.
[26] R.A. Dobbs, R.T. Williams, Anal. Chem. 35 (1963) 1064.
[27] U. Diebold, Surf. Sci. Rep. 48 (2003) 53.
[28] K. Kakiuchi, E. Hosono, H. Imai, T. Kimura, S. Fujihara, J. Cryst. Growth 293 (2006) 541–545.

[29] E. Hosono, S. Fujihara, K. Kakiuchi, H. Imai, J. Am. Chem. Soc. 126 (2004) 7790–7791.
[30] Q. Huang, L. Gao, Chem. Lett. 32 (2003) 638–639.
[31] B. Liu, E.S. Aydil, J. Am. Chem. Soc. 131 (2009) 3985–3990.
[32] Y.H. Jiang, H.B. Yin, Y.M. Sun, H. Liu, L.X. Lei, K.M. Chen, Y.J. Wada, Appl. Surf. Sci. 253 (2007) 9277.
[33] M.N. Tahir, P. Theato, P. Oberle, G. Melnyk, S. Faiss, U. Kolb, A. Janshoff, M. Stepputat, W. Tremel, Langmuir 22 (2006) 5209.
[34] K. Kakiuchi, E. Hosono, H. Imai, T. Kimura, S. Fujihara, J. Cryst. Growth 293 (2006) 541.
[35] J. Yang, S. Mei, J.M.F. Ferreira, P. Norby, S. Quaresmâ, J. Colloid Interface Sci. 283 (2005) 102.
[36] Jeong Ah Chang, Muga Vithal, In Chan Baek, Sang Il Seok, J. Solid State Chem. 182 (2009) 749–756.
[37] P.P. Lottici, D. Bersani, M. Braghini, A. Montenero, J. Mater. Sci. 28 (1993) 177–183.
[38] C.G. Silva, J.L. Faria, J. Mol. Catal. A: Chem. 305 (2009) 147.
[39] C.H. Chiou, C.Y. Wu, R.S. Juang, Chem. Eng. J. 139 (2008) 322.
[40] D.W. Chen, A.K. Ray, Water Res. 32 (1998) 3223.
[41] I.K. Konstantinou, T.A. Albanis, Appl. Catal. B: Environ. 49 (2004) 1.
[42] S. Bekkouche, M. Bouhelassa, N.H. Salah, F.Z. Meghlaoui, Desalination 166 (2004) 355.
[43] N.B. Colthup, J. Opt. Soc. Am. 40 (1950) 397.
[44] N.B. Colthup, L.H. Daly, S.E. Wiberley, Introduction to Infrared and Raman Spectroscopy, 3c ed., Academic, New York, 1990.
[45] D. Lin-Vien, N.B. Colthup, W.G. Fateley, J.G. Grasselli, The Handbook of Infrared and Raman Characteristic Frequencies of Organic Molecules, Academic, New York, 1991.